Stable and dynamic microtubules coordinately shape the myosin activation zone during cytokinetic furrow formation

Victoria E. Foe and George von Dassow

The Center for Cell Dynamics, University of Washington, Friday Harbor, WA 98250

The cytokinetic furrow arises from spatial and temporal regulation of cortical contractility. To test the role microtubules play in furrow specification, we studied myosin II activation in echinoderm zygotes by assessing serine19-phosphorylated regulatory light chain (pRLC) localization after precisely timed drug treatments. Cortical pRLC was globally depressed before cytokinesis, then elevated only at the equator. We implicated cell cycle biochemistry (not microtubules) in pRLC depression, and differential microtubule stability in localizing the subsequent myosin activation. With no microtubules, pRLC accumulation occurred globally instead of equatorially, and loss of just dynamic microtubules increased equatorial pRLC recruitment. Nocodazole treatment revealed a population of stable astral microtubules that formed during anaphase; among these, those aimed toward the equator grew longer, and their tips coincided with cortical pRLC accumulation. Shrinking the mitotic apparatus with colchicine revealed pRLC suppression near dynamic microtubule arrays. We conclude that opposite effects of stable versus dynamic microtubules focuses myosin activation to the cell equator during cytokinesis.

Introduction

Cytokinesis in animal cells entails a transient concentration at the equatorial cortex of F-actin, myosin II, and other proteins. While associated proteins anchor the contractile machinery to the plasma membrane, actomyosin contraction drives furrow ingression. Furrow onset is regulated temporally so that constriction begins only after sister chromatids separate at anaphase, and spatially so that the furrow forms equatorially, between spindle poles, where constriction will bisect the mitotic apparatus, leaving one daughter nucleus on either side of the cleavage plane. It has long been known that the mitotic apparatus, and presumably its microtubules, are key to positioning the cytokinetic furrow (Conrad and Schroeder, 1990; Rappaport 1996).

The small GTPase, Rho, is required for cytokinesis in animal cells (Kishi et al., 1993; Mabuchi et al., 1993; Moorman et al., 1996; Drechsel et al., 1997; O'Connell et al., 1999; Prokopenko et al., 1999; Jantsch-Plunger et al., 2000; Lai et al., 2005; Kamijo et al., 2006; Nishimura and Yonemura, 2006). Rho is cytoplasmic when GDP-bound, but by binding GTP becomes activated and competent to insert into the plasma membrane (DerMardirossian and Bokoch, 2005). Rho activation promotes both F-actin and myosin II recruitment to the cortex. Active Rho binds and activates Diaphanous, which nucleates F-actin polymerization (Watanabe et al., 1997; Afshar et al., 2000). Active Rho also activates Rho kinase, which adds a stimulatory phosphate to myosin regulatory light chain (RLC) and inhibits myosin LC phosphatase, thereby promoting, in two ways, myosin II activity (Kimura et al., 1996; Kawano et al., 1999; Kosako et al., 2000; Royou et al., 2002; Dean and Spudich, 2006). Live imaging in sea urchin embryos showed that active Rho appears at the cell equator immediately before furrowing and that Rho activation continually tracks the midplane of the mitotic apparatus during cleavage (Bement et al., 2005). Rho activation thus appears to be a key intermediary in the mechanism by which the mitotic apparatus signals the cell cortex when and where to assemble the cytokinetic furrow.

Yet, notwithstanding decades of experimentation, debate continues about which parts of the mitotic apparatus specify furrow position and as to whether solely stimulatory signals upregulate contractility at the cell equator, or whether inhibitory

Correspondence to V.E. Foe: vicfoe@u.washington.edu

Abbreviations used in this paper: C phase, cytokinetic phase; DIC, differential interference contrast; GAP, GTPase-activating protein; GEF, guanine exchange factor; ncdz, nocodazole; NEB, nuclear envelope breakdown; pRLC, phosphorylated RLC; RLC, regulatory light chain.

The online version of this article contains supplemental material.

The Rockefeller University Press $30.00
J. Cell Biol. Vol. 183 No. 3 457–470
www.jcb.org/cgi/doi/10.1083/jcb.200807128

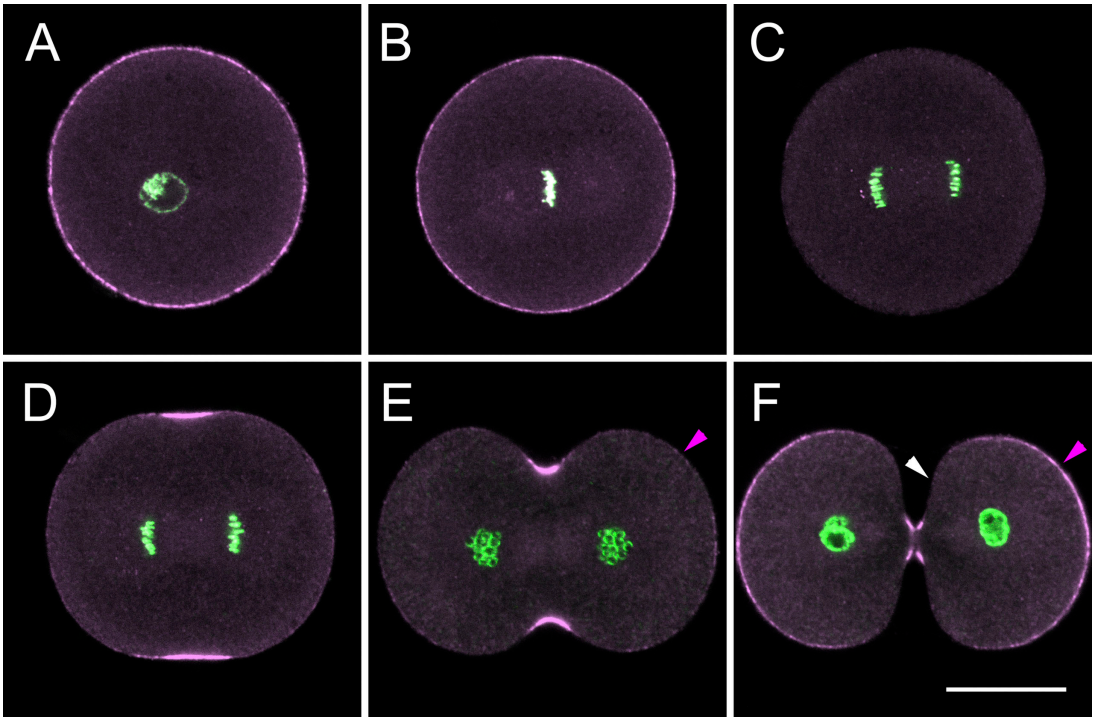

Figure 1. **Cortical pRLC modulation during mitotic progression.** Medial single-section confocal images of first cell cycle *S. purpuratus* zygotes. All cells were identically fixed and stained with Sytox green to reveal nuclei (green) and an antibody to serine19 pRLC (lavender). Identical microscope settings were used throughout for pRLC, but laser intensity was adjusted for Sytox green to make different nuclear condensation states discernable. Lavender arrowheads indicate the polar cortex of the nascent daughter cells, where pRLC reaccumulates before abscission. The white arrowhead indicates pRLC-depleted surface flanking the pRLC-enriched furrow. Bar, 25 µm.

signals down-regulate cortical contractility elsewhere (for reviews see Oegema and Mitchison, 1997; Burgess and Chang, 2005).

Here, we describe the relationship between microtubule stability and myosin II activation, deduced from fixed and stained echinoderm zygotes using precisely timed drug treatments and an antibody that recognizes the serine19-phosphorylated form of myosin RLC, a stimulatory phosphorylation. We show that myosin activation during anaphase is preceded by a global, microtubule-independent signal that transiently depletes the entire cortex of active myosin. We find that, beginning at anaphase onset, a population of nocodazole (ncdz)-resistant astral microtubules forms, whose tips come to be at the right places at the right time to stimulate the observed subsequent accumulation of activated myosin at the cell equator. We show that, at the same time, dynamic microtubules transiently suppress myosin activation outside the furrow zone. We show that myosin accumulation at the cell equator during furrow induction is F-actin independent but Rho dependent, and that astral microtubule stabilization occurs without Rho activation.

Results

Global myosin dephosphorylation is the prelude to furrow specification

To study myosin II regulation during cytokinesis, we studied localization of serine19-phosphorylated myosin RLC (pRLC) in zygotes of three echinoids: the purple urchin *Strongylocentrotus purpuratus*, the green urchin *Strongylocentrotus droebachiensis*, and the sand dollar *Dendraster excentricus*. These zygotes are large (80, 160, and 125 µm in diameter, respectively). They showed similar pRLC localization patterns, with some differences in timing.

Figs. 1 and 2 show single-section confocal micrographs of fixed *S. purpuratus* zygotes stained to reveal pRLC and chromatin in Fig. 1, and pRLC and microtubules in Fig. 2. pRLC was present in a uniform cortical layer during all of interphase, prophase, and metaphase, and disappeared from the cortex during anaphase (Fig. 1, A–C). In *S. purpuratus* zygotes, the interval between anaphase onset and furrow onset was 7–8 min (10–11°C), and pRLC reached its nadir in approximately two thirds of that time. Anaphase pRLC loss was not synchronous from cell to cell, but proceeded uniformly within each single cell; specifically, it had no spatial correlation with where or when elongating astral microtubules first made cortical contact (see control cells in Fig. 2, D–F). During late anaphase, although the cortex elsewhere remained pRLC-depleted, RLC phosphorylation began in a faint, often discontinuous, equatorial band. By early telophase, pRLC had localized in a sharply focused cortical ring circumscribing the entire equator, with higher pRLC levels than the cortex had during interphase, prophase, or metaphase (Fig. 1, D and E). The pRLC-rich equator began as broad and saddle-shaped (Fig. 2, G–I) and, during ingression, narrowed to leave pRLC just on the furrow floor (Fig. 2, J and K). Before abscission completed, pRLC staining in the furrow became undetectable (e.g., Fig. 2 L). Approximately when ingression reached its midpoint, the inward-facing surfaces of the nascent cells abruptly lost pRLC

staining, and remained flat and pRLC-depleted through abscission (Fig. 1 F, white arrowhead). Daughter cells re-adhered along these pRLC-depleted faces (not depicted), while at the same time pRLC returned gradually to the polar cortex of the nascent daughter cells (Fig. 1, E and F, lavender arrowheads). This highly polarized pRLC distribution is retained throughout interphase in the blastomeres (unpublished data), replacing the prior uniform cortical distribution of pRLC seen throughout interphase in the spherical zygote.

Comparing Fig. 1 to Fig. S1 (available at http://www.jcb.org/cgi/content/full/jcb.200807128/DC1) shows that in the cell interior, where RLC staining showed little serine19 phosphorylation, myosin heavy chain was equally abundant at all mitotic stages. In contrast, myosin heavy chain recruited to and dissociated from the cell cortex in approximate synchrony with RLC serine19 phosphorylation, although the two probes did not maintain exact proportionality. Specifically, myosin in the furrow was more heavily phosphorylated than cortical myosin elsewhere. And thinning (or complete dissociation) of cortical myosin heavy chain from the anaphase cortex was not evident until late anaphase, lagging RLC dephosphorylation by about 2 min.

A population of stable astral microtubules forms during anaphase; their tips at the cortex coincide temporally and spatially with cortical pRLC accumulation

Ncdz readily enters urchin embryonic cells, and by binding tubulin dimers, renders these unable to polymerize. Thus, after a cell spends, e.g., 5 min in 20 μM ncdz, the only microtubules remaining will be those that during this interval did not depend on continued growth to avoid catastrophe (i.e., because they are in some way protected from dynamic instability). Complete depolymerization of a cell's microtubules implies that all were sufficiently dynamic to depolymerize during the 5-min exposure to ncdz, and because ncdz had inactivated the unpolymerized tubulin, none could grow back. To examine microtubule stability, we immersed precisely staged zygotes in 20 μM ncdz, then, at defined intervals thereafter, transferred them directly from ncdz into fixative, subsequently staining to reveal microtubules and pRLC. In each two-cell panel of Fig. 2, the bottom cell was fixed after 5 min in 20 μM ncdz, whereas the upper cell is a same-stage untreated sibling, identically fixed and stained.

During interphase and prophase, all microtubules were dynamically unstable: untreated cells contained large numbers of microtubules, but after 5 min in ncdz, no microtubules remained (Fig. 2, A and B, compare top and bottom cells). Ncdz treatment of metaphase cells showed that only kinetochore microtubules (known to be bundled; Mastronarde et al., 1993) survived 5 min in ncdz (Fig. 2 C, cyan arrowheads). Fig. S2 (available at http://www.jcb.org/cgi/content/full/jcb.200807128/DC1) shows that near complete depolymerization of interphase microtubules had already occurred by two min in 20 μM ncdz. Fig. S3 shows the same depolymerization time for astral microtubules in metaphase cells (Fig. S3, A–C).

During anaphase, astral microtubules elongated until their tips contacted the cortex, reaching the poles before the equator (Fig. 2, D–F, control cells). Anaphase astral microtubules aimed everywhere, and most were ncdz sensitive. But among the large number of dynamic microtubules was a subset of ncdz-resistant astral microtubules (Fig. 2, D–G) extending from the periphery of the centrosphere. (In echinoid cells, the centrosome swells enormously during anaphase, and in this state is called a "centrosphere." Note the enlarging circle from which microtubules project in Fig. 2 [D–G] control cells. Then, beginning at telophase and continuing until the next anaphase, microtubules are nucleated from a small centrosome. Note how in Fig. 2 [A–C and H–L] control cells astral microtubules project to a point.) Progressively older anaphase cells showed more and longer stable astral microtubules, and those on the side of the centrosphere nearest to the chromosomes appeared earliest and, on average, grew longest. Fig. S4 (available at http://www.jcb.org/cgi/content/full/jcb.200807128/DC1) shows in the larger *S. droebachiensis* zygote the wavelike birth of stable astral microtubules around the centrosphere perimeter. During late anaphase, high-level pRLC appeared first at the cell equator when and where the tips of ncdz-resistant astral microtubules met the cortex (Fig. 2 G). Elsewhere however, where microtubules near the cortex were mostly dynamic, pRLC remained attenuated (Fig. 2 G). 3D reconstructions of serial confocal sections of purple urchin zygotes treated with ncdz at furrow initiation often showed pRLC puncta precisely where individual stable microtubule tips contacted the cortex (Video 1).

During telophase, furrow constriction gathered ncdz-resistant astral microtubules from opposite poles into an initially loose bundle, and the gathered plus ends of the stable microtubules remained associated with the pRLC-rich furrow floor throughout ingression (Fig. 2, H–J). During abscission, the bundled stable microtubules gradually decreased in number and formed discrete antiparallel arrays (Fig. 2, K and L).

The ncdz-resistant bundled kinetochore microtubules, which ended on the metaphase chromosomes, moved apart at anaphase onset, when chromatids separated, then shortened as chromatids moved poleward (Fig. 2, C–E, ncdz-treated cells, cyan arrowheads). As the kinetochore bundles shortened, a less organized array of ncdz-resistant microtubules, which Mastronarde et al. (1993) called "interpolar microtubules," appeared, seemingly nucleated from the same region that previously nucleated kinetochore microtubules (Fig. 2, E–J, red arrowheads). Interpolar microtubules were dimmer than kinetochore bundles but brighter than the stable astral microtubules (Fig. 2, D–F), which is consistent with EM tomographic studies of PtK_1 cells that show them to be small bundles (Mastronarde et al., 1993). The EM study also showed that interpolar microtubules became increasingly organized into antiparallel arrays with their opposite-polarity counterparts from the opposite pole, which is consistent with our observations in urchin zygotes (Fig. 2, K and L). In our fixed preparations, the region of presumed antiparallel plus end overlap showed no tubulin staining (where the Mastronarde et al., [1993] EM study showed microtubules), presumably because in this region, interpolar microtubules are so densely coated with proteins that they resist antibody binding (Fig. 2, E–J). (Nota bene, we use "interpolar microtubules" rather than "central spindle" to designate the bipolar array of interdigitating nonkinetochore microtubules that forms between anaphase and telophase centrosomes because we think both this array and the ncdz-resistant subset of astral microtubules described in the previous

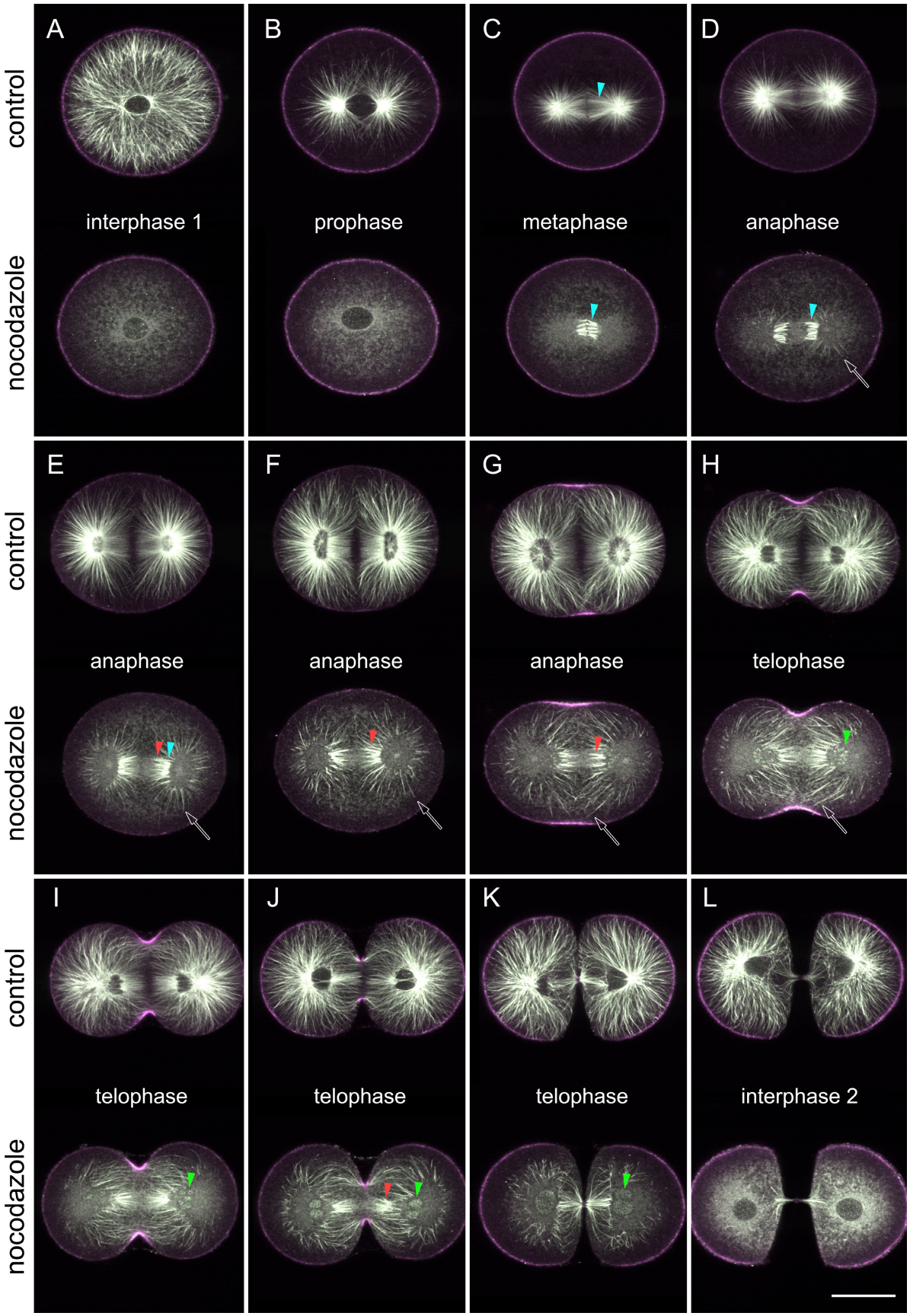

Figure 2. **pRLC elevation at the equatorial cortex correlates with proximity to ncdz-resistant astral microtubule tips.** Medial single-section confocal images of *S. purpuratus* zygotes, from one female, synchronously fertilized and allowed to develop to the stage indicated, then fixed and stained for pRLC (lavender) and tubulin (white). In each two-cell panel, the bottom cell was treated with 20 μM ncdz for 5 min before fixation (11°C), whereas the top

paragraph concentrate the protein complex called centralspindlin. We prefer not to designate one of two centralspindlin-decorated arrays "the" central spindle.) The presumed minus ends of interpolar and ncdz-resistant astral microtubules terminated at the edge of the centrosphere (Fig. 2, E–J), with which they remained associated until they broke down during abscission (Fig. 2, K–L, ncdz-treated cells).

The small centrosome that formed inside each swollen centrosphere in early telophase nucleated only dynamic astral microtubules (Fig. 2, G and H, control cells show the transition from centrosphere to centrosome). Reforming nuclei (Fig. 2, H–K, ncdz-treated cells, green arrows) moved away from the minus ends of the interpolar microtubules toward the new centrosome.

The global myosin dephosphorylation that precedes furrowing does not require the presence of dynamic anaphase microtubules

Figs. 3 and S3 document, for *S. purpuratus* zygotes, the sensitivity of the cortex to extended ncdz exposure as a function of mitotic phase and passage of chronological time. Fig. 3 shows nuclei and pRLC; Fig. S3 shows pRLC and microtubules. pRLC levels in interphase and early metaphase were insensitive to prolonged exposure to ncdz (Fig. 3, A–D and E–H), which indicates that microtubules are not involved in pRLC regulation during these mitotic phases.

Late metaphase cells lost cortical pRLC in ncdz at the same chronological time they would have had they entered anaphase normally (compare Fig. 3, K and N, with Fig. 3 Q). Fig. S3 shows that after 2 min in ncdz, metaphase astral microtubules had largely depolymerized (Fig. S3, A and B), whereas kinetochore fibers sometimes persisted as long as 16 min in ncdz, although pole-to-pole distance gradually decreased (likely because of kinetochore microtubule flux; Wittmann et al., 2001). It also shows that cells lost cortical pRLC well after the disappearance of all astral microtubules in cells that had not separated their chromatids (Fig. S3, F–H). We conclude that to trigger cortical clearing of pRLC, cells must advance past a microtubule-requiring metaphase event (perhaps the spindle checkpoint, as clearing did not occur in cells transferred to ncdz during early metaphase), and that global myosin dephosphorylation, normally coincident with anaphase microtubule outgrowth, not only does not require anaphase astral microtubules but can occur in cells arrested in metaphase.

Cells transferred into ncdz during late metaphase were often able to separate sister chromatids (Fig. 3, M and N), presumably because kinetochore microtubules resist rapid depolymerization (Fig. S3, A–H). Cells that separated chromatids in the presence of ncdz underwent a high-level global RLC activation at the same chronological time that control cells with microtubules showed high-level equatorial pRLC recruitment (Fig. 3, O and Y); cells that decondensed their chromosomes without chromatid separation did not (Fig. 3 L). We infer that the high-level RLC phosphorylation that sets the stage for cleavage requires some brief action by kinetochore microtubules at anaphase onset, and that it takes 5–10 min (10–11°C) after anaphase onset for this large cell to recover from its prior RLC dephosphorylation and become competent to elevate cortical pRLC.

Ncdz treatment during early-to-mid anaphase blocked furrowing (Fig. 3, Q–T) or produced broad furrows that regressed (Fig. 3, U–X); the same treatment during late anaphase did not prevent abscission (Fig. 3, Y–Σ), which is in agreement with earlier studies (Beams and Evans 1940; Swann and Mitchison 1953; Hamaguchi 1975; Mullins and Snyder 1981). Fig. S3 shows that "ncdz-resistant" anaphase microtubules gradually depolymerized in cells transferred into ncdz during early (Fig. S3, "1 anaphase") or late anaphase (Fig. S3, "3 anaphase"). Cells that completed division had retained at least a few stable microtubules in their constricted furrow (Fig. S3, W and X).

Dynamic microtubules inhibit cortical RLC phosphorylation during furrow induction

Figs. 3 and S3 show that loss of dynamic microtubules during anaphase resulted in a dramatic increase in equatorial pRLC (e.g., Fig. 3 W). That ncdz increased both pRLC concentration and furrow width was evident in 3D projections: compare the control zygote in Fig. 4 A to ncdz-treated cells in Fig. 4 (B and C). (Fig. 4, D–F, shows in sectional view pRLC and microtubules in those cells whose pRLC-stained surfaces are shown in A–C.) In control zygotes (developing without ncdz), at the end of anaphase, we frequently observed low level pRLC accumulation at the equator, where neither stable nor dynamic microtubules had made equatorial contact (Fig. 4, G and J); this corresponded to the phase when, in cells lacking all microtubules, pRLC rose globally. Culturing *S. purpuratus* zygotes in 1 mM colchicine reduced the overall size of the mitotic apparatus without blocking mitotic progression. Fig. 4 (H and K, and I and L) shows zygotes grown in 1 mM colchicine, at late anaphase and early telophase, respectively. With no microtubules contacting the equator, pRLC appeared in a diffuse, broader-than-normal equatorial band whose shape was a negative imprint of proximity to the astral microtubules. But it is notable that, at this same phase of the mitotic cycle, equatorial pRLC accumulation is dramatically higher if stable astral microtubule tips contact the cortex (Fig. 4, A–F). We conclude that both dynamic and stable microtubules contribute to shaping the furrow zone; proximity to dynamic microtubules correlated with a local inhibition of the normal telophase pRLC elevation, whereas proximity to stable microtubule tips correlated with a potent local pRLC stimulation.

PRLC localization to the furrow requires active Rho but not F-actin

Differential interference contrast (DIC) movies of urchin embryos show no large-scale cortical flow. To determine whether

cell was fixed without drug treatment. Arrows indicate the ncdz-resistant astral microtubules that appear during anaphase and elongate; pRLC accumulates to high levels near their tips (G). Cyan arrowheads mark bundled kinetochore microtubules (C–E), red arrowheads indicate interpolar microtubules (E–G and J), and green arrowheads indicate reforming telophase nuclei (H–K). Identical microscope settings were used throughout for pRLC. Laser intensity was adjusted to ensure visibility of microtubule tips, and higher laser intensity was used for the ncdz-treated cells (thus, e.g., stable kinetochore microtubules, represented by cyan arrowheads in C, appear brighter in ncdz-treated than in control cells). Bar, 20 μm.

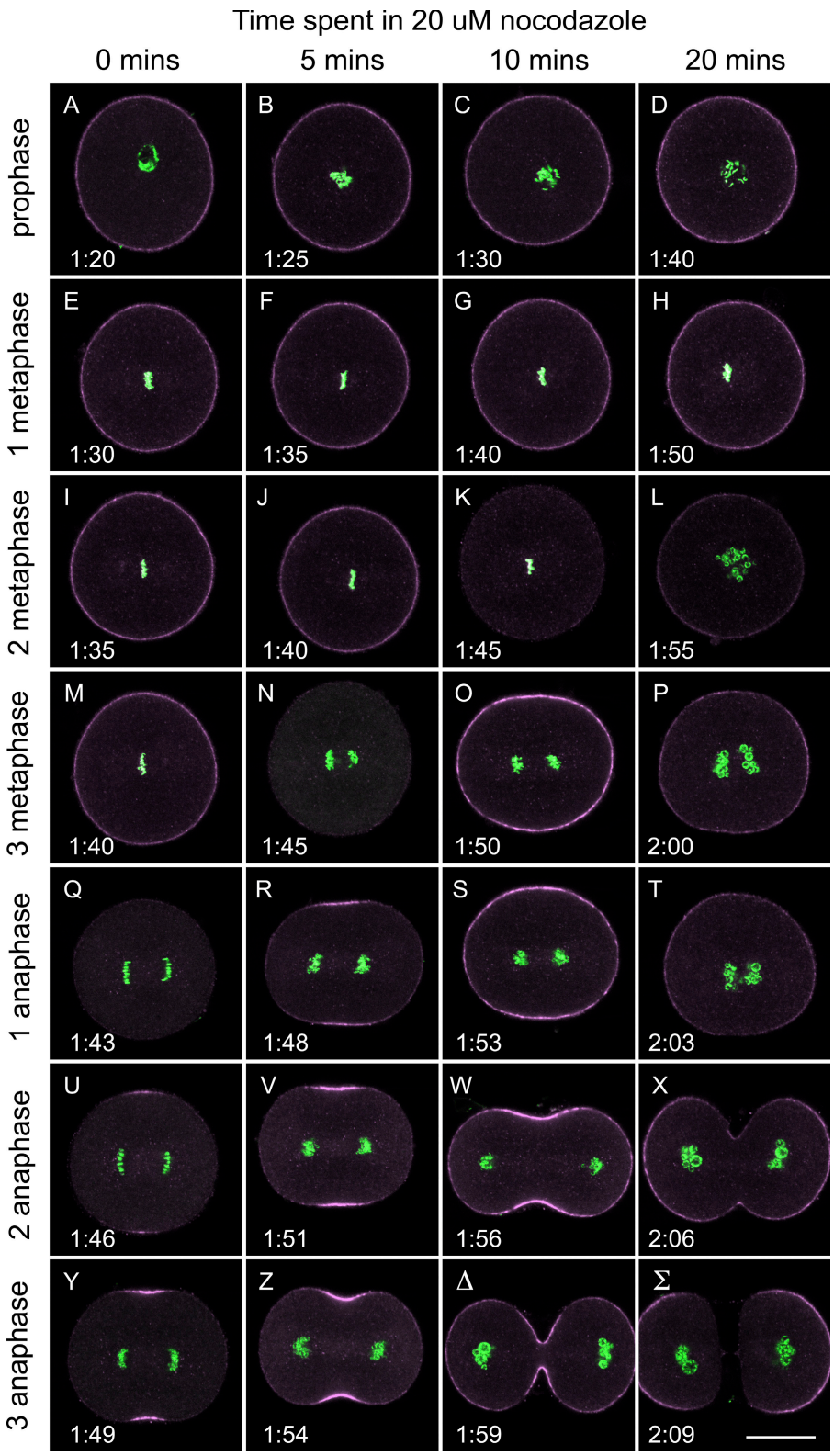

Figure 3. **Prolonged ncdz treatment reveals complex gating of cortical pRLC levels.** Medial single-section confocal images of *S. purpuratus* zygotes, from one female, fertilized synchronously, cultured to the stage shown, and immersed in 20 µM ncdz for the period indicated, then identically fixed and stained to reveal pRLC (lavender) and DNA (green). Identical microscope settings were used throughout for pRLC, but laser intensity was adjusted for different DNA condensation states. The number in each panel indicates chronological age (11.5°C) defined by the interval between sperm addition and the moment when that cell was transferred into fixative (e.g., 1:35 means fixed 1 h, 35 min after fertilization). The left column (0 min in 20 µM ncdz) shows the normal progression of control cells developing without ncdz. Each row displays cells that have spent 5, 10, and 20 min in ncdz, having been transferred into ncdz at the same time the control cells in the same row were transferred into fixation medium. Each panel shows one example of the most abundant phenotype for the specified time point, typically the only phenotype, determined by examining a slide containing >100 cells for the time point in question. Bar, 25 µm.

pRLC recruitment to the cell equator was dependent in any way on F-actin, we bathed sand dollar zygotes in 20 µM latrunculin B 20 min before nuclear envelope breakdown (NEB), then fixed these cells and untreated siblings of the same age when the latter were beginning to furrow. Although the latrunculin-treated cells never furrowed, mitosis continued (spindle poles separated and nuclei reformed). The fine-scale organization of pRLC was abnormal but, strikingly, latrunculin-treated cells accumulated a sharply defined equatorial band of pRLC even though F-actin had been lost from the entire cortex (Fig. 5). We conclude that recruitment of myosin to the equator requires neither F-actin itself nor any actomyosin-driven process.

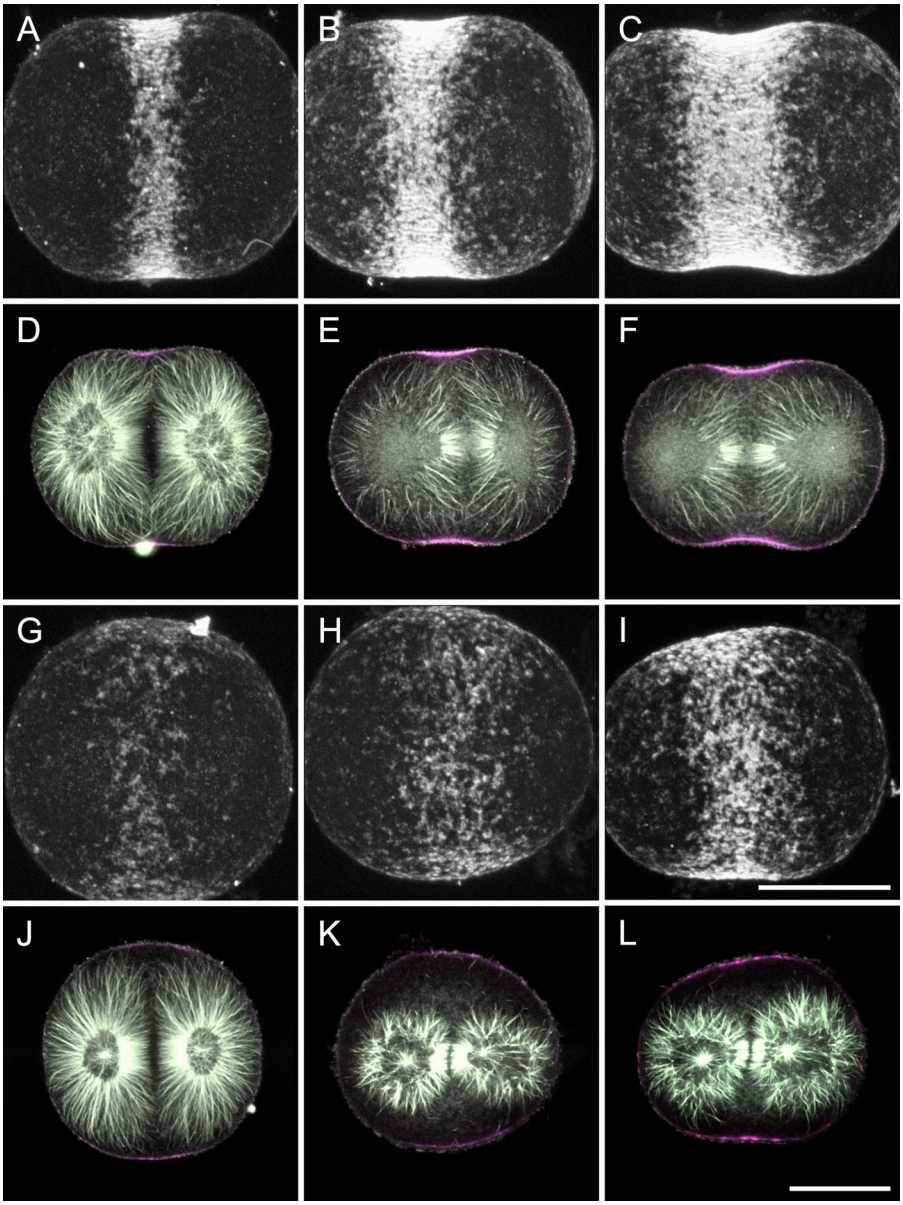

Figure 4. **The cortex reacts differently to the proximity of stable vs. dynamic microtubules.** *S. purpuratus* zygotes: (A–C and G–I) Projections of 71 serial confocal sections (0.5 µm apart) revealing surface views of pRLC (white). Immediately below each surface projection are medial sectional views of the same cell (D–F and J–L) showing microtubules (white) and pRLC (lavender). (A–C) Telophase zygotes after 0, 4, and 8 min in ncdz (12°C) from the same preparations as Fig. S3, Q, S, and U, respectively (available at http://www.jcb.org/cgi/content/full/jcb.200807128/DC1). (G) An anaphase zygote, developing normally without ncdz, fixed just before elongating microtubules contacted the equator. (H and I) Late anaphase zygotes cultured in 1 mM colchicine. The same confocal microscope settings were used throughout for pRLC, but adjusted to optimize microtubule images. Bars, 25 µm; Surface projections are shown at 1.3× higher magnification than midsection micrographs.

C3 transferase inactivates Rho irreversibly by ADP-ribosylation (Aktories and Hall, 1989). We injected C3 (to an intracellular concentration of ~8 ng/µl) into *D. excentricus* zygotes during interphase, 30–75 min after fertilization. Under the temperature regimen used, noninjected controls initiated cleavage ~90 min after fertilization. Sand dollar zygotes injected at NEB often completed the next division. Zygotes injected with C3 at least 15 min before NEB developed a fine-scale cortical crenation, remained spherical, and did not furrow. These cells paused in interphase, and the interphase nuclei became abnormally swollen. Then, beginning when their noninjected siblings were undergoing second cleavage, the C3-injected zygotes underwent an apparently normal first nuclear division, without cytokinesis (Video 2, available at http://www.jcb.org/cgi/content/full/jcb.200807128/DC1). Thereafter, mitosis continued on a normal schedule but with no sign of cortical contractility.

In contrast to noninjected controls (Fig. 6, A–C), C3-injected sand dollar zygotes traversed telophase with no detectable pRLC at the equatorial cortex (Fig. 6, D and E), reentered interphase without pRLC reappearing at the cell poles (Fig. 6 F), and still lacked cortical pRLC even three cycles later (Fig. 6 G).

Stable microtubules form without active Rho but the interpolar array does not compact

To test whether Rho acts upstream or downstream of anaphase microtubule stabilization, we injected C3 into *D. excentricus* zygotes, let these cells develop to the desired mitotic phase, treated them for 5 min with 20 µM ncdz, then fixed and stained them to reveal stable microtubules. In parallel, we fixed and stained ncdz-treated sibling zygotes that had not been C3-injected. With or without the capacity to activate Rho, during anaphase, kinetochore bundles shortened, and the stable astral microtubule array formed and grew out (Fig. 7, A and B, and E and F). Normally, stable astral microtubules growing from the hemisphere of the centrosphere nearest the chromosomes gradually became longer,

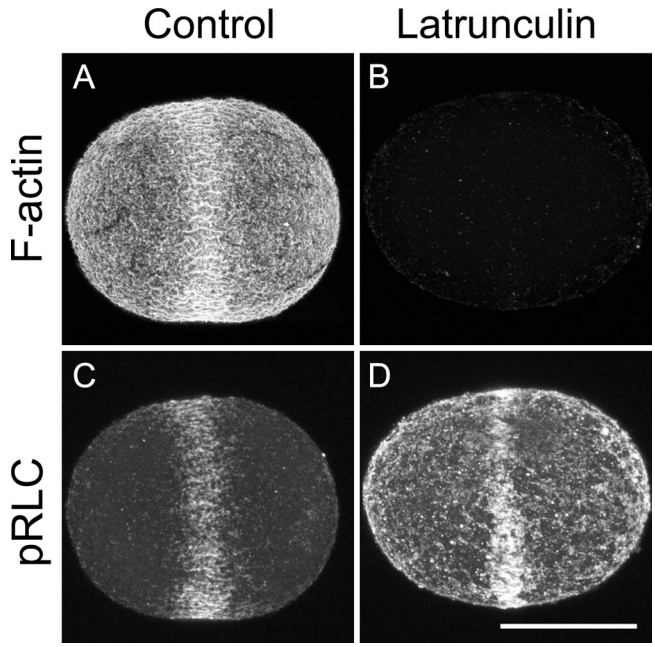

Figure 5. **Equatorial recruitment of pRLC does not require F-actin.** Surface views made from projecting 64 serial confocal sections (0.5 µm apart) of two sibling *D. excentricus* zygotes. Cells in B and D were cultured in 20 µM latrunculin (13°C); cells in A and C were cultured without latrunculin. Both cells were fixed during telophase. A and B show F-actin (stained with Bodipy FL phallacidin); C and D show pRLC. Identical preparation protocols and microscope settings were used for cells in A and B, and C and D, respectively. Bar, 35 µm.

whereas those extending poleward decreased in length and number (Fig. 7 C; also see Fig. 2). In C3-injected cells, stable microtubules extending poleward remained numerous and did not shorten. Microtubules extending toward the equator, although often longer than poleward microtubules, frequently became disorganized (Fig. 7 G). In *D. excentricus*, the interpolar array is less dense than in *S. purpuratus*, but it is similarly ncdz resistant (Fig. 7, B–D, arrowheads). In C3-injected cells, ncdz-resistant interpolar microtubules grew out at anaphase, but compaction did not occur, and by mid-telophase, this array was gone (Fig. 7, G and H). With or without active Rho, all ncdz-resistant microtubules were gone by late interphase (not depicted).

Discussion

A global cortical relaxation clears the stage for furrow specification

We found in urchin zygotes that a short-lived global dephosphorylation of myosin RLC at serine19, leading to loss of myosin II from the entire cortex, immediately precedes furrow formation. Myosin dephosphorylation normally took until mid-anaphase to complete, but we show that it can be made to occur earlier, in zygotes arrested in metaphase by ncdz. We conclude that precleavage RLC dephosphorylation requires neither the presence of astral microtubules nor anaphase onset. In agreement with our findings in urchins, Werner et al. (2007) recently found that in *Caenorhabditis elegans*, nonmuscle myosin dissociates from the cortex during metaphase, and that postponing metaphase exit by depleting embryos of the proteosome regulatory subunit extends the period of myosin inactivation. Similarly, in the syncytial *Drosophila melanogaster* embryo, a gradual global loss of cortical myosin, which normally reaches it nadir in anaphase (Foe et al., 2000), was found to be set in motion at metaphase, by cdc2 (Royou et al., 2002). Perhaps precleavage myosin dephosphorylation is stimulated by mitosis-specific activation of myosin phosphatase, which in cultured rat cells is regulated by cdc2/cyclinB-dependent phosphorylation of the myosin phosphatase targeting subunit (Totsukawa et al., 1999).

In principle, it makes sense to "wipe the cortex clean" of active myosin as a prelude to furrow induction and to erase interphase myosin accumulations (stress fibers, focal adhesions, etc.), which might impede furrow initiation and whose components will need to regroup to cleave the cell. In echinoid zygotes, which lack those specialized structures, clearing the cortex of active myosin appears to be half of a two-part mechanism that ensures the cell poles are relaxed during furrow initiation.

In situ RLC phosphorylation, not cortical flow, initially recruits myosin to the furrow

In urchin embryos, Rho activation in a sharply focused zone at the cell equator anticipates, and is essential for, furrowing (as in other cell types), and the Rho activation zone will form without F-actin (Bement et al., 2005). Studies in *D. melanogaster* S2 cells using amino acid substitution mimics of various RLC phosphorylation states showed that serine19 phosphorylation is necessary for myosin recruitment to the equatorial cortex, and that maintenance of this RLC phosphorylation state is the only essential role for Rho kinase during cytokinesis (Dean and Spudich, 2006). That myosin recruitment to the cytokinetic furrow can occur independently of F-actin has been shown for *Dictyostelium discoideum* (Yumura and Uyeda, 1997; Zang and Spudich, 1998), *D. melanogaster* S2 (Dean et al., 2005), and cultured mammalian cells (Kamijo et al., 2006; Nishimura and Yonemura. 2006; Zhou and Wang, 2008). We show here that suppressing Rho activation in urchin zygotes blocks equatorial serine19 phosphorylation of RLC and furrowing, that reducing F-actin to undetectable levels with latrunculin blocks furrowing but does not prevent equatorial pRLC accumulation, and that in normal cells, myosin heavy chain recruitment and furrow initiation follows RLC phosphorylation at serine19. Thus, the simplest explanation for myosin recruitment to the nascent cytokinetic furrow is that myosin is activated locally, by RLC phosphorylation at serine19, in response to local Rho activation.

Obviously, once a band of activated myosin has formed around the cell equator, one expects this myosin to assemble into bipolar filaments and (in a normal cell with no latrunculin present) to engage F-actin and pull any existing cortical actin meshwork toward the furrow, a process computer modeling shows would drive a self-amplifying realignment of the tension-producing cortical actomyosin (White and Borisy, 1983). But, what is critical to the discussion that follows is that local de novo RLC phosphorylation, and not actomyosin-based cortical flow, initially recruits myosin to the nascent cytokinetic furrow.

Anaphase hands control of the cortex over to the mitotic apparatus

Shuster and Burgess (2002) found, in both the sand dollar *Echinarachnius parma* and the sea urchin *Lytechinus pictus*, that

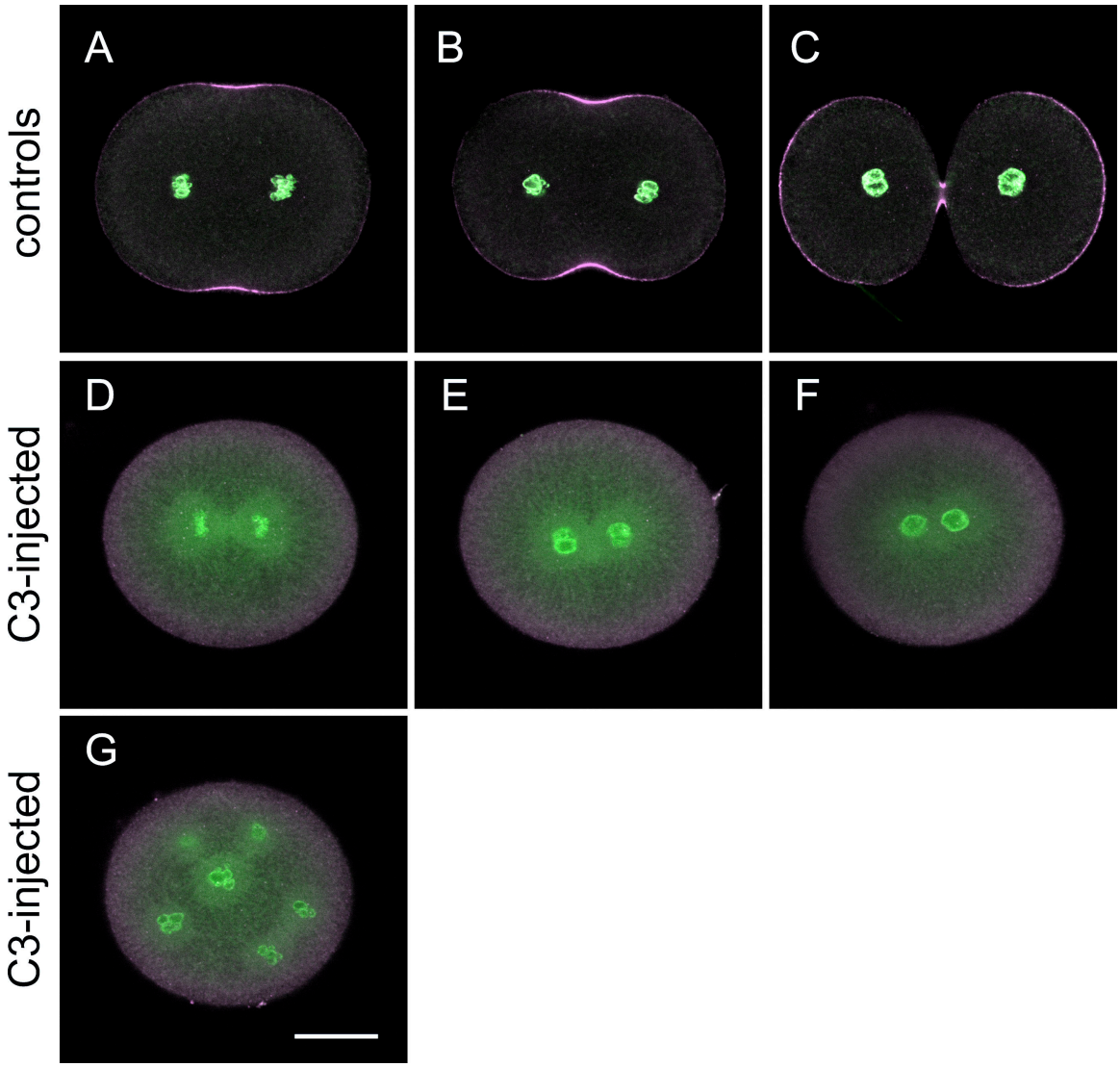

Figure 6. **Recruitment of pRLC to the cell cortex requires Rho activity.** Single medial confocal sections of fixed and stained *D. excentricus* embryos at first (A–F) and third (G) telophase. (A–C) Noninjected controls. (D–G) Zygotes injected with C3-transferase >15 min before NEB. (D–G) Coinjected fixable FITC-dextran labels the cytoplasm (to mark injected cells). A and D, B and E, and C and F are matched by mitotic phase. All cells were stained to show pRLC (lavender) and nuclei (green). Bar, 25 μm.

manipulating the mitotic apparatus into proximity with the cortex could precociously induce a furrow beginning as early as 3.5 min after anaphase onset, but would not induce furrowing in metaphase cells, nor in cells microinjected with MAD2 protein, which prevents metaphase exit. Canman et al. (2000) showed that PtK_1 cells lacking microtubules (because of ncdz treatment before mitosis), when forced to enter anaphase, became rampantly contractile, and remained so for ~50 min. They termed this 50-min period the cytokinetic phase ("C phase") and interpreted it as that postmitotic period when the cell cortex is competent to make a cytokinetic furrow should the appropriate stimulus tell it where to do so. Ncdz washout and microtubule regrowth during C-phase resulted in furrowing in a third of the cells, implicating microtubules in providing the missing stimulus (Canman et al., 2000). This disorganized C-phase contractility induced by microtubule loss was recently shown to require Rho activation (Niiya et al., 2005; Kamijo et al., 2006). In agreement with these studies, our timed ncdz treatments of urchin zygotes showed that although the cortex of interphase, prophase, and early metaphase cells were unaffected by microtubule depolymerization, after a short refractory period, the anaphase cortex became locally sensitive to the proximity of microtubules. Importantly, we found that the cortex becomes differently sensitive to stable versus dynamic microtubules.

Dynamic microtubules maintain polar relaxation during C phase

Exposing urchin zygotes to concentrated ncdz immediately before the metaphase–anaphase transition (which did not block chromosome separation and exit from mitosis because bundled kinetochore microtubules resisted rapid depolymerization) led, after a delay of 7–10 min (10–11°C), to pRLC elevation over the entire cortex in cells that by then lack all microtubules. This global pRLC elevation occurred during late anaphase/early telophase, precisely

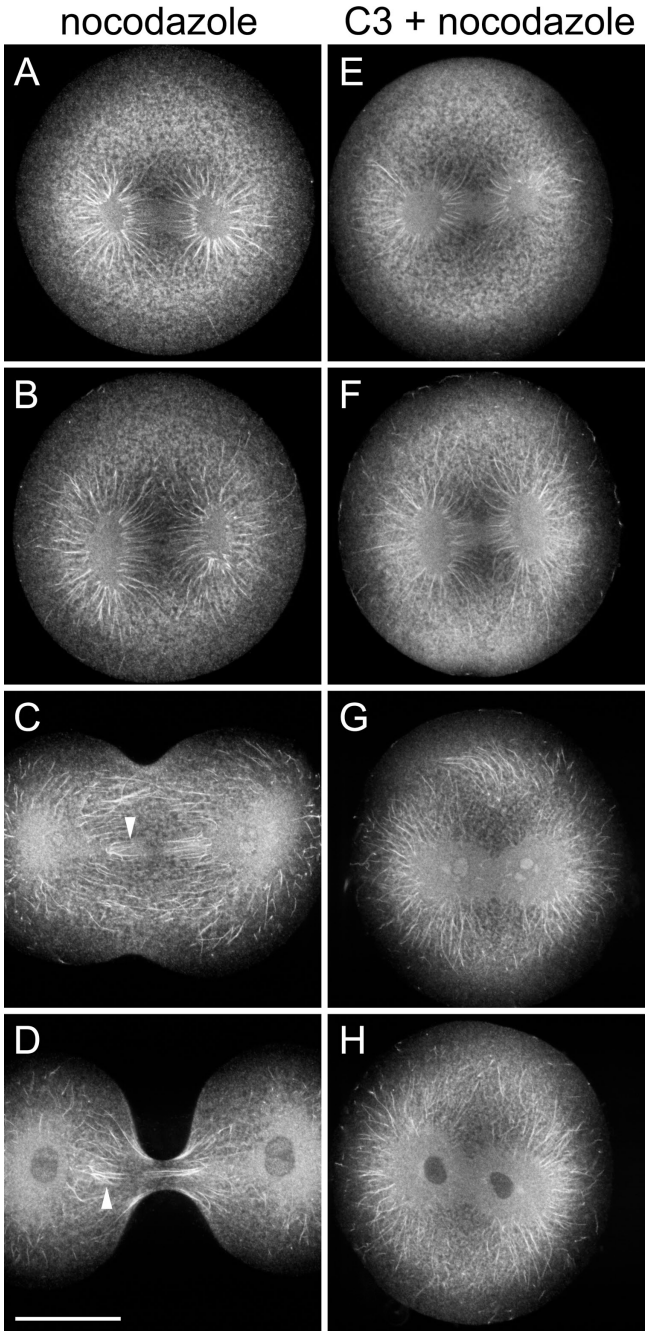

Figure 7. **Stable astral microtubules form without Rho activity.** Medial single-section confocal images of *D. excentricus* zygotes. (A–D) Cells were treated with 20 µM ncdz for 5 min (12°C), then fixed and stained to reveal ncdz-resistant microtubules. (E–H) Cells were injected at least 15 min before NEB with C3, which induced an extended interphase. C3-injected cells were monitored under bright field until they resumed mitosis, transferred at the desired stage into 20 µM ncdz for 5 min (12°C), then fixed and stained identically to the noninjected cells. Shown are anaphase (A and B, and E and F), telophase (C and G), and early interphase (D and H). Arrowheads indicate condensed interpolar array, which is absent from same-stage C3-injected cells. Loss of dynamic astral microtubules frequently permits the interpolar array to slip sideways during ingression (as in D). Bar, 25 µm.

when controls showed high-level pRLC recruitment to the cell equator. Our studies show that the astral microtubules that contact the cell poles are dynamic and normally suppress pRLC recruitment outside the furrow zone. Murthy and Wadsworth (2008) have similarly shown in adherent LLC-Pk1 cells that loss of dynamic microtubules during anaphase activates unfocused, fluctuating contractility outside the furrow, which they show depends on mislocalized Rho and Rho kinase activation. Treating urchin zygotes with 1 mM colchicine produced an intact but smaller-than-normal mitotic apparatus, in which, by telophase, microtubules had not reached the future equator and astral microtubules contacted a smaller-than-usual area of cortex. Beginning at late anaphase and continuing through telophase, cortical pRLC reappeared everywhere, except where the reduced mitotic asters made cortical contact, revealing that the inhibitory influence of dynamic microtubules is local. Genetic and pharmacological perturbations have recently shown the same thing in *C. elegans* (Werner et al., 2007). In effect, these experiments confirm the existence of a polar relaxation mechanism of the sort Wolpert (1960) postulated could induce furrowing.

Among proteins implicated in cytokinesis, there is consensus that three are key to regulating Rho during cytokinesis, and all three concentrate at furrows: a kinesin-6 family motor protein (called MKLP1 in mammals, Pavarotti in flies, and ZEN-4 in worms; Adams et al., 1998; Powers et al., 1998; Raich et al., 1998; Matuliene and Kuriyama, 2002), a Rho guanine exchange factor (GEF) that activates Rho (ECT2 in mammals, Pebble in flies, and LET-21 in worms; Prokopenko et al., 1999; Tatsumoto et al., 1999; Kimura et al., 2000; Kim et al., 2005; Yuce et al., 2005), and a Rho GTPase-activating protein (GAP), which binds and recruits the Rho GEF, and the actin- and myosin-binding protein Anillin to the furrow (called MgcRacGAP in mammals, Tumbleweed or RacGAP50C in flies, and CYK-4 in worms; Jantsch-Plunger et al., 2000; Hirose et al., 2001; Minoshima et al., 2003; Somers and Saint, 2003; Zavortink et al., 2005; Gregory et al., 2008). We refer henceforth to these cytokinetic Rho pathway proteins as RhoGEF, RhoGAP, and MKLP1, and use "centralspindlin" to denote the MKLP1/RhoGAP oligomer, which forms at anaphase (Mishima et al., 2002).

Centralspindlin binds RhoGEF (probably weakly), and its MKLP1 component gives centralspindlin the ability to bind microtubules (Somers and Saint, 2003; Yuce et al., 2005; Zhao and Fang, 2005; Chalamalasetty et al., 2006; D'Avino et al., 2006; Kamijo et al., 2006; Nishimura and Yonemura, 2006). Additionally, its pleckstrin homology (PH) domains target RhoGEF to the plasma membrane (Chalamalasetty et al., 2006). Thus, during C phase, centralspindlin bound to microtubules likely competes with the plasma membrane for RhoGEF, which may explain why C phase without microtubules hyperactivates the cortex, and why the proximity to microtubule arrays depresses RhoGEF, and hence RLC phosphorylation, in the adjacent cortex (see Odell and Foe, on p. 471 of this issue). In the following section, we review evidence indicating that the same cytokinesis-specific Rho activation pathway causes both furrow stimulation and polar relaxation, a hypthesis also suggested by Murthy and Wadsworth (2008). However, we don't yet know whether urchins additionally have a centralspindlin-independent mechanism for inducing cortical relaxation, which many cell types clearly do (e.g., Hime and Saint, 1992; Foe et al., 2000; Werner et al., 2007).

Stable microtubules stimulate myosin recruitment to the cortex

Canman et al. (2003) analyzed microtubule behavior in live cultured mammalian cells, and found that in both monopolar and normal bipolar cells, although most C-phase astral microtubules were dynamic, a subset formed stable contacts with the cortex, and furrows formed where high numbers of stable astral microtubules made cortical contact. In *D. melanogaster* spermatocytes, furrowing occurred where a distinct population of astral microtubules (the "peripheral central spindle") formed antiparallel bundles beneath the cell surface, and in *D. melanogaster* S2 cells, where the tips of certain astral microtubules made cortical contact (Inoue et al., 2004); sensitivity to ncdz was not explored. In flat adherent mammalian cultured cells, Murthy and Wadsworth (2008) found that furrows formed adjacent to ncdz-resistant interpolar microtubules. In urchin zygotes, which are large (80–160 μm) cells, we found that high levels of pRLC appeared during late anaphase when and where the tips of ncdz-resistant astral microtubule approached the cortex. In urchin zygotes, interpolar microtubules formed and stabilized rapidly after mitotic exit, and during the several minutes between anaphase onset and furrow initiation, the ncdz-resistant astral microtubules became increasingly longer, whereas their presumed minus ends remained anchored at the edge of the centrosphere. This indicates either that they are stable from birth and retain their stability as they grow out, or that stabilization propagates in a minus-to-plus end direction along ncdz-sensitive microtubules. Stable astral microtubules extending toward the equator became longer and more numerous than those extending poleward; this patterned stabilization did not require microtubule contact with chromosomes, and at least initially, did not require bundling with opposite-polarity microtubules, active Rho, equatorial RLC phosphorylation, or furrowing. However, in C3-injected cells, the interpolar array did not compact, or persist, and the stable astral array formed but lost its polarized organization. This implies a late requirement for something necessitating active Rho, perhaps Diaphanous or pRLC to compact the interpolar array (Giansanti et al., 1998), and possibly feedback from the furrow itself, as proposed by Hu et al. (2008). pRLC accumulation in the incipient furrow occurred where the tips of apparently single stable astral microtubules contacted the cortex. Confocal images do not distinguish single from bundled parallel microtubules, but furrow stimulation clearly preceded assembly of the stable astral microtubules into antiparallel arrays, assembly of which did occur during abscission.

In urchin zygotes, the cortical stimulation associated with stable microtubule tips occurred after myriad dynamic microtubules had already contacted the poles without causing myosin activation there. Moreover, stable microtubules must have the ability to override any inhibitory influence dynamic microtubules have because many dynamic microtubules also contact the equatorial cortex during or soon after furrow initiation. Were stabilization acting simply to block the inhibitory influence of dynamic microtubules (e.g., Dechant and Glotzer, 2003), then preventing all microtubule contact with the equator should elicit the same level activation seen when stable microtubules contact the equator. Instead, we observed much higher levels of pRLC accumulation when and where the tips of stable microtubules tips underlay the cortex (Fig. 4).

Our observations thus support the hypothesis, first advanced by Canman et al. (2003), that stable microtubules stimulate, whereas dynamic microtubules suppress, cortical contractility during C phase. Consistent with a two-handed furrow specification mechanism, recent studies in *C. elegans* (Bringmann and Hyman, 2005; Baruni et al., 2008) elegantly show the existence of two furrow-positioning signals: the first and weaker signal emanating from the astral microtubule arrays acted to position a furrow midway between asters; the second and dominant signal induced a furrow over the spindle midzone. Depletion of centralspindlin components eliminated the spindle midzone furrow-stimulating signal and reduced, but did not altogether eliminate, the astral signal (Bringmann and Hyman, 2005). This demonstrates that the signal that stimulates myosin recruitment above the mitotic apparatus midzone in worms acts through centralspindlin, and the signal from the asters, which acts by suppressing myosin recruitment to the poles (Werner et al., 2007), does as well (although, as already noted, when centralspindlin is missing, the polar weakening signal proceeds by a redundant mechanism). Our finding that loss of dynamic astral microtubules during early anaphase (by ncdz treatment) expands and intensifies equatorial pRLC recruitment near stable astral microtubules implies that in urchins, likewise, cortex stimulation and inhibition act through the same proteins (see also Murthy and Wadsworth, 2008).

Microtubule stabilization and centralspindlin

The ncdz-resistant microtubules we found in urchin zygotes included the interpolars and a subset of astral microtubules. Nishimura and Yonemura (2006) observed heavy accumulations of centralspindlin at the midzone of the interpolar array and on the tips of a subset of astral microtubules in cleaving HeLa cells; Rho and pRLC accumulation occurred where centralspindlin-coated astral or interpolar microtubules contacted the cortex. It remains to be shown that astral microtubules with centralspindlin decorating their tips are specifically ncdz resistant. And if they are, it remains to be determined what is a cause and what is an effect.

Shannon et al. (2005) found that C-phase furrows develop not only where naturally occurring stable microtubules contact the cortex, but also where microtubules stabilized artificially by taxol contact the cortex, with even a single taxol-stabilized microtubule being sufficient to induce transient furrowing. This strongly suggests that, whatever its cause, stability by itself, rather than some other property differentiating naturally occurring ncdz-resistant from ncdz-sensitive astral microtubules, is key to cortical stimulation.

It is worth noting that in the flat cells studied by Murthy and Wadsworth (2008), it is apparently the ncdz-resistant interpolar array that stimulates furrowing (see also Cao and Wang, 1996; Nishimura and Yonemura, 2006). In *C. elegans*, although centralspindlin heavily decorates the antiparallel overlap of the bipolar interpolar microtubule array, it has not been shown on the tips of astral microtubules (though it does accumulate on the furrow cortex; Verbrugghe and White, 2007). Thus, in some

cells, stimulation of the equatorial cortex may occur by diffusion of centralspindlin to the cortex from a concentrated source on the interpolar array (while dynamic astral microtubules block stimulation of the poles), rather than by delivery via stable astral microtubules. This less precise means of delivering a stimulus to the cortex may suffice to specify a sharply bounded furrow in cells where cortical flow can rapidly amplify small cortical actomyosin nonuniformities into focused contractions (as occurs in these cell types; Werner et al., 2007; Murthy and Wadsworth, 2008).

Conclusion

We detect in urchin zygotes four distinct regulatory processes that combine to ensure a sharply bounded equatorial myosin II localization zone at furrow onset: (1) a global myosin dephosphorylation/inactivation induced during late metaphase that remains in effect during early anaphase; followed by (2) a potentially global elevation in a cell's potential to phosphorylate myosin RLC, set in motion at anaphase onset, and that will actually occur globally and cause global contractility beginning in late anaphase unless focused by the mitotic apparatus; (3) suppression of myosin phosphorylation/activation near dynamic astral microtubule arrays; (4) and strong myosin phosphorylation/activation where stable microtubules approach the cortex. We show that either stable or dynamic microtubules can cause pRLC elevation at the equator relative to the poles: only dynamic astral microtubules produce a sloppy weak equatorial band, whereas only stable astral microtubules cause an abnormally concentrated and broad equatorial band. In a companion paper, we use an agent-based computer model to demonstrate how stable and dynamic microtubules might oppositely affect kinesin-based delivery of Rho regulators to the cortex and show how these two microtubule populations could act together to specify a spatially confined furrow induction signal in the face of diffusion (Odell and Foe, 2008).

Materials and methods

Animals and embryos

S. purpuratus were collected intertidally at Clallam Bay, WA, and kept in submerged cages. *D. excentricus* were collected intertidally at Crescent Beach, Eastsound, WA, and kept on sand in flowing seawater tanks. *S. droebachiensis* were collected subtidally near San Juan Island, WA, and kept in flowing seawater tanks. Eggs and zygotes were cultured in coarse-filtered natural seawater at 9–13°C (in a flowing seawater table). Adults were spawned by intracoelomic injection of 0.55 M KCl. Eggs were collected by inverting a female over a beaker of seawater. Sperm was collected dry. For fertilization, sperm was diluted ~1:10,000 into 250 ml of seawater containing eggs. Fertilization synchrony was checked by looking for elevated fertilization membranes 2 min after adding sperm. We fertilized purple and green urchin eggs in seawater containing 1 mM 3-amino-triazole (3-ATA; Sigma Aldrich) to prevent hardening of fertilization membranes. To strip off soft fertilization membranes, we passed eggs through Nitex mesh (two to three times through 66–73-µm mesh for *S. purpuratus* zygotes; one to two times through 153-µm mesh for *S. droebachiensis*). Newly fertilized eggs secrete hyaline, and to prevent stripped eggs from clumping, we delayed stripping until secretion stops (30 min for purple urchin eggs and 60 min for green urchin eggs). 3-ATA does not work on *D. excentricus*, but their membranes remain soft enough to strip up to 14 min after fertilization, by which time hyaline secretion has abated; we stripped these by passing them once or twice through 130 µm Nitex mesh. *D. excentricus* eggs intended for injection were stripped while hyaline secretion was still ongoing, 7–8 min after fertilization. If transferred immediately to glass, eggs stick sufficiently to remain in place for injection yet can be detached without damage.

Microinjection of C3

We transferred stripped *D. excentricus* zygotes by mouth pipette to a 35-mm Petri dish (MatTek) with 14 mm microwell and No. 1.5 cover glass bottom containing a small volume of seawater, positioning eggs in single file across the glass bottom. Injection needles were pulled on a micropipette puller (Model P-97 Flaming-Brown; Sutter Instrument Co.) from borosilicate-with-filament glass (outer diameter, 1.0 mm; inner diameter 0.50 mm; Sutter Instrument Co.). Eggs were injected using a hanging joystick micromanipulator (MO-202D; Narishige) on an inverted microscope (Eclipse TS 100; Nikon), equipped with a thermoelectric cooling stage (HE-101S; Dagan Corporation) and a pneumatic microinjector (PicoSpritzer III; Parker Instrumentation).

The C3 injection solution was 1 µl of 1 µg/µl C3 exotransferase (Cytoskeleton Inc.) + 0.4 µl of 3 mM DTT (freshly made) + 0.4 µl of 5× injection buffer (500 mM potassium glutamate, pH 7.4, 250 mM KCl, and 50 mM Hepes) + 0.2 µl 25 mg/ml fixable 70-kD TRITC Dextran (Invitrogen). Needles were back-filled, mounted at 30°, and broken to a tip diameter of <5 µm. We injected ~2% of cell volume. Injected cells were checked for cleavage with a fluorescence dissecting microscope (SMZ 1500; Nikon), and nuclear cycle progression was monitored on an inverted microscope (Eclipse TS 100) with a cooling stage. Cells were released from the injection dish with a pipette stream of seawater, concentrated in the center of the dish by swirling, and a measured volume of eggs plus seawater was transferred into ncdz or fixative.

The same C3 concentration that blocked cytokinesis in sand dollar zygotes, injected into purple urchin zygotes during interphase, caused cell lysis during mitosis. For this reason, we used *D. excentricus* for C3 studies. ncdz treatment causes high background tubulin staining in *D. excentricus* (e.g., Figs. 7 and S2).

Treatment with ncdz, latrunculin, and colchicine

Ncdz (Sigma-Aldrich) from a frozen solution in DMSO was diluted into seawater to 25 µM. 1 ml of seawater with eggs was rapidly mixed into 4 ml of 25 µM ncdz solution to a final concentration of 20 µM. 20 µM ncdz is at least five times more concentrated than needed to elicit the effects reported herein. Latrunculin B and colchicine (Sigma-Aldrich) were added similarly to 20 µM and 1 mM, respectively. Incubations were at seawater temperature (9–12°C, as indicated in legends) in 6-well culture plates.

Fixation

We fixed cells in 100 mM Hepes, pH 6.9, 50 mM EGTA, 10 mM $MgSO_4$, 2% formaldehyde, 0.2% glutaraldehyde, 0.2% acrolein, 0.2% Triton X-100, and 400 mM–1 M dextrose. For good preservation of cortex and microtubule plus ends, we adjusted dextrose concentration for species and local salinity to minimize shrinkage or swelling (we usually used 600 mM for *D. excentricus* and *S. droebachiensis*, and 800 mM for *S. purpuratus*). Hepes and EGTA stocks were made from free acid titrated with KOH to pH 6.9 (rather than from the Na salt because Triton X-100 permeabilization in a high Na concentration leads to cortex rupture at anaphase). We made up the fixative from stock solutions the day of use and chilled to seawater temperature. We omitted 10% volume of H_2O from the fixative, then added one tenth volume of eggs in seawater to the fixative and mixed thoroughly. We fixed for 70 min with slow agitation at room temp, washed three times with PBS with 0.1% Triton X-100 (PBT), then stored in PBT at 4°C. To minimize glutaraldehyde-induced autofluorescence, we treated before staining with 0.1% $NaBH_4$ in PBS (made fresh). We let eggs sit uncapped until bubbling ceased (1–2 h), washed once in PBT, blocked them overnight with 5% normal goat serum in PBT, then stained them.

Staining

Antibody penetration into large glutaraldehyde-fixed cells requires long incubations (1 d for purple urchins and 2–3 d for sand dollars and green urchins, at room temperature with occasional agitation). Antibody rinses were performed in PBT twice rapidly, then overnight at 4°C. We used either 1:8,000 mouse anti–α-tubulin (DM1A clone; GE Healthcare) or 1:4,000 rat anti–α-tyr-tubulin (YL 1/2 clone; Immunologicals Direct); both antibodies stain dynamic and stable microtubules, but the images shown used YL 1/2, which gave lower background staining. We used anti-myosin heavy chain antibody prepared against purple urchin egg myosin II (a gift from D. Burgess, Boston College, Chestnut Hill, MA; Yabkowitz and Burgess, 1987) at 1:750, and an antibody to the serine19-phosphorylated form of myosin RLC (Cell Signaling Technology) at 1:250. We used Alexa-conjugated secondary antibodies (Invitrogen) at 1:750.

To stain chromatin, we incubated antibody-stained cells in PBT in 55 µg/ml RNase A (Sigma-Aldrich) for 45 min at 37°C, then in 1 µl/ml Sytox Green (Invitrogen) for >4 h at room temperature. We stored antibody and chromatin-stained cells in PBS at 4°C before mounting. We stained F-actin

with 5 µl/ml BODIPY-FL phallacidin (from a 1 U/µl stock in DMSO; Invitrogen) in PBT for 1–2 h, rinsed for 30–45 min (long washes destain F-actin), and then mounted immediately.

Specimen mounting and imaging

We pipetted cells dispersed in PBS onto poly-lysine–coated slides (freshly dipped in 0.05% poly-L-lysine (Sigma-Aldrich) with 0.2% Photoflow (Kodak), then air dried between two shims of aluminum tape (110-µm thick 3M 425 tape; Scotch). The slide was dehydrated through 70%, 85%, 95%, 100%, and 100% isopropanol for 50 s per step, then through three 20-min changes in Murray clear (2:1 benzyl benzoate/benzyl alcohol). Dehydration shrinks eggs isometrically 25–35%. We use a No. 0 coverslip, sealing it first with 5-min epoxy, then with nail varnish (Wet-N-Wild). All confocal imaging was with a laser scanning confocal microscope (Radiance 2000; Bio-Rad Laboratories) on a microscope (E800; Nikon) with a 60× 1.4 NA oil Plan Apo objective (Nikon) using LaserSharp image acquisition software (Bio-Rad Laboratories). In each multipanel figure, zygotes were from the same female and cultured at the same temperature (see legends), and pRLC was imaged using identical microscope settings (those settings chosen so the full grayscale range of the detector were used at early telophase, when pRLC staining is brightest). Figures were laid out using Photoshop version 9.0.2 (Adobe). No nonlinear adjustments or convolution filters were applied. Maximum projections (Video 1) were made from confocal stacks using Stax (G.M. Odell; http://www.celldynamics.org/celldynamics/downloads/index.html). Time-lapse films (Video 2) were made on a WL standard DIC microscope (Carl Zeiss, Inc.) using a Neofluar 25× 0.8 Imm Korr objective (Carl Zeiss, Inc.), a charge-coupled device camera (C2400-77; Hamamatsu), and BTV Pro software (Ben Software), then compressed using QuickTime (Apple).

Online supplemental material

Fig. S1 shows *S. purpuratus* zygotes stained to reveal myosin II heavy chain. Fig. S2 shows the timing of interphase microtubule loss in *D. excentricus* zygotes exposed to 20 µM ncdz. Fig. S3 shows, in *S. purpuratus* zygotes, that sensitivity to ncdz of both cortical pRLC and microtubules changes with cell cycle phase. Fig. S4 shows, in *S. droebachiensis* zygotes, that the outgrowth of stable astral microtubule begins on the side of the centrosome closest to the chromosomes. Video 1 is a projection of confocal images showing that in the incipient furrow of *S. purpuratus* zygote, puncta of pRLC appear on the cortex near the tips of ncdz-resistant microtubules. Video 2 is a DIC time-lapse video of two *D. excentricus* zygotes injected with C3 transferase, showing arrest in interphase then eventual resumption of nuclear division cycles without cytokinesis. Online supplemental material is available at http://www.jcb.org/cgi/content/full/jcb.200807128/DC1.

We thank David Burgess for the generous gift of anti-myosin antibody prepared against *S. purpuratus* egg myosin II heavy chain and Yvonne Beckham for help in manuscript preparation. We thank Bill Bement, Julie Canman, Karen Oegema, and Garrett Odell for reading our manuscript and providing many helpful suggestions.

We gratefully acknowledge the Seaver Institute, whose support enabled us to begin this work (grant "Using 3D Microscopic Imaging to Study Mechanisms of Cell Division, Cell Shape Change and Cell Movement"), and the National Institute of General Medical Sciences, whose support of the Center for Cell Dynamics (grant 1 P50 GM066050) allowed us to bring it to fruition.

Submitted: 23 July 2008
Accepted: 5 September 2008

References

Adams, R.R., A.A. Tavares, A. Salzberg, H.J. Bellen, and D.M. Glover. 1998. Pavarotti encodes a kinesin-like protein required to organize the central spindle and contractile ring for cytokinesis. *Genes Dev.* 12:1483–1494.

Afshar, K., B. Stuart, and S.A. Wasserman. 2000. Functional analysis of the *Drosophila* diaphanous FH protein in early embryonic development. *Development.* 127:1887–1897.

Aktories, K., and A. Hall. 1989. Botulinum ADP-ribosyltransferase C3: a new tool to study low molecular weight GTP-binding proteins. *Trends Pharmacol. Sci.* 10:415–418.

Baruni, J.K., E.M. Munro, and G. von Dassow. 2008. Cytokinetic furrowing in toroidal, binucleate, and anucleate cells in *C. elegans* embryos. *J. Cell Sci.* 121:306–316.

Beams, H.W., and T.C. Evans. 1940. Some effects of colchicine upon the first cleavage in *Arbacia punctulata. Biol. Bull.* 79:188–198.

Bement, W.M., H.A. Benink, and G. von Dassow. 2005. A microtubule-dependent zone of active RhoA during cleavage plane specification. *J. Cell Biol.* 170:91–101.

Bringmann, H., and A.A. Hyman. 2005. A cytokinesis furrow is positioned by two consecutive signals. *Nature.* 436:731–734.

Burgess, D.R., and F. Chang. 2005. Site selection for the cleavage furrow at cytokinesis. *Trends Cell Biol.* 15:156–162.

Canman, J.C., D.B. Hoffman, and E.D. Salmon. 2000. The role of pre- and post-anaphase microtubules in the cytokinesis phase of the cell cycle. *Curr. Biol.* 10:611–614.

Canman, J.C., L.A. Cameron, P.S. Maddox, A. Straight, J.S. Tirnauer, T.J. Mitchison, G. Fang, T.M. Kapoor, and E.D. Salmon. 2003. Determining the position of the cell division plane. *Nature.* 424:1074–1078.

Cao, L.G., and Y.L. Wang. 1996. Signals from the spindle midzone are required for the stimulation of cytokinesis in cultured epithelial cells. *Mol. Biol. Cell.* 7:225–232.

Chalamalasetty, R.B., S. Hummer, E.A. Nigg, and H.H. Sillje. 2006. Influence of human Ect2 depletion and overexpression on cleavage furrow formation and abscission. *J. Cell Sci.* 119:3008–3019.

Conrad, G.W., and T.E. Schroeder. 1990. Cytokinesis: mechanisms of furrow formation during cell division. New York Academy of Sciences, New York. 328 pp.

D'Avino, P.P., M.S. Savoian, L. Capalbo, and D.M. Glover. 2006. RacGAP50C is sufficient to signal cleavage furrow formation during cytokinesis. *J. Cell Sci.* 119:4402–4408.

Dean, S.O., and J.A. Spudich. 2006. Rho kinase's role in myosin recruitment to the equatorial cortex of mitotic *Drosophila* S2 cells is for myosin regulatory light chain phosphorylation. *PLoS ONE.* 1:e131.

Dean, S.O., S.L. Rogers, N. Stuurman, R.D. Vale, and J.A. Spudich. 2005. Distinct pathways control recruitment and maintenance of myosin II at the cleavage furrow during cytokinesis. *Proc. Natl. Acad. Sci. USA.* 102:13473–13478.

Dechant, R., and M. Glotzer. 2003. Centrosome separation and central spindle assembly act in redundant pathways that regulate microtubule density and trigger cleavage furrow formation. *Dev. Cell.* 4:333–344.

DerMardirossian, C., and G.M. Bokoch. 2005. GDIs: central regulatory molecules in Rho GTPase activation. *Trends Cell Biol.* 15:356–363.

Drechsel, D.N., A.A. Hyman, A. Hall, and M. Glotzer. 1997. A requirement for Rho and Cdc42 during cytokinesis in *Xenopus* embryos. *Curr. Biol.* 7:12–23.

Foe, V.E., C.M. Field, and G.M. Odell. 2000. Microtubules and mitotic cycle phase modulate spatiotemporal distributions of F-actin and myosin II in *Drosophila* syncytial blastoderm embryos. *Development.* 127:1767–1787.

Giansanti, M.G., S. Bonaccorsi, B. Williams, E.V. Williams, C. Santolamazza. 1998. Cooperative interactions between the central spindle and the contractile ring during *Drosophila* cytokinesis. *Genes Dev.* 12:396–410.

Gregory, S.L., S. Ebrahimi, J. Milverton, W.M. Jones, A. Bejsovec, and R. Saint. 2008. Cell division requires a direct link between microtubule-bound RacGAP and Anillin in the contractile ring. *Curr. Biol.* 18:25–29.

Hamaguchi, Y. 1975. Microinjection of colchicine into sea urchin eggs. *Dev. Growth Differ.* 17:111–117.

Hime, G., and R. Saint. 1992. Zygotic expression of the pebble locus is required for cytokinesis during the post-blastoderm mitoses of *Drosophila*. *Development.* 114:165–171.

Hirose, K., T. Kawashima, I. Iwamoto, T. Nosaka, and T. Kitamura. 2001. MgcRacGAP is involved in cytokinesis through associating with mitotic spindle and midbody. *J. Biol. Chem.* 276:5821–5828.

Hu, C.K., M. Coughlin, C.M. Field, and T.J. Mitchison. 2008. Cell polarization during monopolar cytokinesis. *J. Cell Biol.* 181:195–202.

Inoue, Y.H., M.S. Savoian, T. Suzuki, E. Mathe, M.T. Yamamoto, and D.M. Glover. 2004. Mutations in *orbit/mast* reveal that the central spindle is comprised of two microtubule populations, those that initiate cleavage and those that propagate furrow ingression. *J. Cell Biol.* 166:49–60.

Jantsch-Plunger, V., P. Gonczy, A. Romano, H. Schnabel, D. Hamill, R. Schnabel, A.A. Hyman, and M. Glotzer. 2000. CYK-4: A Rho family GTPase activating protein (GAP) required for central spindle formation and cytokinesis. *J. Cell Biol.* 149:1391–1404.

Kamijo, K., N. Ohara, M. Abe, T. Uchimura, H. Hosoya, J.S. Lee, and T. Miki. 2006. Dissecting the role of Rho-mediated signaling in contractile ring formation. *Mol. Biol. Cell.* 17:43–55.

Kawano, Y., Y. Fukata, N. Oshiro, M. Amano, Y. Nakamura, M. Ito, F. Matsumura, M. Inagaki, and K. Kaibuchi. 1999. Phosphorylation of myosin-binding subunit (MBS) of myosin phosphatase by Rho-kinase in vivo. *J. Cell Biol.* 147:1023–1038.

Kim, J.E., D.D. Billadeau, and J. Chen. 2005. The tandem BRCT domains of Ect2 are required for both negative and positive regulation of Ect2 in cytokinesis. *J. Biol. Chem.* 280:5733–5739.

Kimura, K., M. Ito, M. Amano, K. Chihara, Y. Fukata, M. Nakafuku, B. Yamamori, J. Feng, T. Nakano, K. Okawa, et al. 1996. Regulation of myosin phosphatase by Rho and Rho-associated kinase (Rho-kinase). *Science.* 273:245–248.

Kimura, K., T. Tsuji, Y. Takada, T. Miki, and S. Narumiya. 2000. Accumulation of GTP-bound RhoA during cytokinesis and a critical role of ECT2 in this accumulation. *J. Biol. Chem.* 275:17233–17236.

Kishi, K., T. Sasaki, S. Kuroda, T. Itoh, and Y. Takai. 1993. Regulation of cytoplasmic division of *Xenopus* embryo by rho p21 and its inhibitory GDP/GTP exchange protein (rho GDI). *J. Cell Biol.* 120:1187–1195.

Kosako, H., T. Yoshida, F. Matsumura, T. Ishizaki, S. Narumiya, and M. Inagaki. 2000. Rho-kinase/ROCK is involved in cytokinesis through the phosphorylation of myosin light chain and not ezrin/radixin/moesin proteins at the cleavage furrow. *Oncogene.* 19:6059–6064.

Lai, S.L., C.N. Chang, P.J. Wang, and S.J. Lee. 2005. Rho mediates cytokinesis and epiboly via ROCK in zebrafish. *Mol. Reprod. Dev.* 71:186–196.

Mabuchi, I., Y. Hamaguchi, H. Fujimoto, N. Morii, M. Mishima, and S. Narumiya. 1993. A rho-like protein is involved in the organisation of the contractile ring in dividing sand dollar eggs. *Zygote.* 1:325–331.

Mastronarde, D.N., K.L. McDonald, R. Ding, and J.R. McIntosh. 1993. Interpolar spindle microtubules in PTK cells. *J. Cell Biol.* 123:1475–1489.

Matuliene, J., and R. Kuriyama. 2002. Kinesin-like protein CHO1 is required for the formation of midbody matrix and the completion of cytokinesis in mammalian cells. *Mol. Biol. Cell.* 13:1832–1845.

Minoshima, Y., T. Kawashima, K. Hirose, Y. Tonozuka, A. Kawajiri, Y.C. Bao, X. Deng, M. Tatsuka, S. Narumiya, W.S.J. May, et al. 2003. Phosphorylation by aurora B converts MgcRacGAP to a RhoGAP during cytokinesis. *Dev. Cell.* 4:549–560.

Mishima, M., S. Kaitna, and M. Glotzer. 2002. Central spindle assembly and cytokinesis require a kinesin-like protein/RhoGAP complex with microtubule bundling activity. *Dev. Cell.* 2:41–54.

Moorman, J.P., D.A. Bobak, and C.S. Hahn. 1996. Inactivation of the small GTP binding protein Rho induces multinucleate cell formation and apoptosis in murine T lymphoma EL4. *J. Immunol.* 156:4146–4153.

Mullins, J.M., and J.A. Snyder. 1981. Anaphase progression and furrow establishment in nocodazole-arrested PtK1 cells. *Chromosoma.* 83:493–505.

Murthy, K., and P. Wadsworth. 2008. Dual role for microtubules in regulating cortical contractility during cytokinesis. *J. Cell Sci.* 121:2350–2359.

Niiya, F., X. Xie, K.S. Lee, H. Inoue, and T. Miki. 2005. Inhibition of cyclin-dependent kinase 1 induces cytokinesis without chromosome segregation in an ECT2 and MgcRacGAP-dependent manner. *J. Biol. Chem.* 280:36502–36509.

Nishimura, Y., and S. Yonemura. 2006. Centralspindlin regulates ECT2 and RhoA accumulation at the equatorial cortex during cytokinesis. *J. Cell Sci.* 119:104–114.

O'Connell, C.B., S.P. Wheatley, S. Ahmed, and Y.L. Wang. 1999. The small GTP-binding protein rho regulates cortical activities in cultured cells during division. *J. Cell Biol.* 144:305–313.

Odell, G.M., and V.E. Foe. 2008. An agent-based model contrasts opposite effects of dynamic and stable microtubules on cleavage furrow positioning. *J. Cell Biol.* 183:471–483.

Oegema, K., and T.J. Mitchison. 1997. Rappaport rules: cleavage furrow induction in animal cells. *Proc. Natl. Acad. Sci. USA.* 94:4817–4820.

Powers, J., O. Bossinger, D. Rose, S. Strome, and W. Saxton. 1998. A nematode kinesin required for cleavage furrow advancement. *Curr. Biol.* 8:1133–1136.

Prokopenko, S.N., A. Brumby, L. O'Keefe, L. Prior, Y. He, R. Saint, and H.J. Bellen. 1999. A putative exchange factor for Rho1 GTPase is required for initiation of cytokinesis in *Drosophila*. *Genes Dev.* 13:2301–2314.

Raich, W.B., A.N. Moran, J.H. Rothman, and J. Hardin. 1998. Cytokinesis and midzone microtubule organization in *Caenorhabditis elegans* require the kinesin-like protein ZEN-4. *Mol. Biol. Cell.* 9:2037–2049.

Rappaport, R. 1996. Cytokinesis in animal cells. Cambridge University Press, New York. 386 pp.

Royou, A., W. Sullivan, and R. Karess. 2002. Cortical recruitment of nonmuscle myosin II in early syncytial *Drosophila* embryos: its role in nuclear axial expansion and its regulation by Cdc2 activity. *J. Cell Biol.* 158:127–137.

Shannon, K.B., J.C. Canman, C. Ben Moree, J.S. Tirnauer, and E.D. Salmon. 2005. Taxol-stabilized microtubules can position the cytokinetic furrow in mammalian cells. *Mol. Biol. Cell.* 16:4423–4436.

Shuster, C.B., and D.R. Burgess. 2002. Transitions regulating the timing of cytokinesis in embryonic cells. *Curr. Biol.* 12:854–858.

Somers, W.G., and R. Saint. 2003. A RhoGEF and Rho family GTPase-activating protein complex links the contractile ring to cortical microtubules at the onset of cytokinesis. *Dev. Cell.* 4:29–39.

Swann, M.M., and J.M. Mitchison. 1953. Cleavage of sea-urchin eggs in colchicine. *J. Exp. Biol.* 30:506–514.

Tatsumoto, T., X. Xie, R. Blumenthal, I. Okamoto, and T. Miki. 1999. Human ECT2 is an exchange factor for Rho GTPases, phosphorylated in G2/M phases, and involved in cytokinesis. *J. Cell Biol.* 147:921–928.

Totsukawa, G., Y. Yamakita, S. Yamashiro, H. Hosoya, D.J. Hartshorne, and F. Matsumura. 1999. Activation of myosin phosphatase targeting subunit by mitosis-specific phosphorylation. *J. Cell Biol.* 144:735–744.

Verbrugghe, K.J.C., and J.G. White. 2007. Cortical centralspindlin and Ga have parallel roles in furrow initiation in early *C. elegans* embryos. *J. Cell Sci.* 120:1772–1778.

Watanabe, N., P. Madaule, T. Reid, T. Ishizaki, G. Watanabe, A. Kakizuka, Y. Saito, K. Nakao, B.M. Jockusch, and S. Narumiya. 1997. p140mDia, a mammalian homolog of *Drosophila* diaphanous, is a target protein for Rho small GTPase and is a ligand for profilin. *EMBO J.* 16:3044–3056.

Werner, M., E. Munro, and M. Glotzer. 2007. Astral signals spatially bias cortical myosin recruitment to break symmetry and promote cytokinesis. *Curr. Biol.* 17:1286–1297.

White, J.G., and G.G. Borisy. 1983. On the mechanisms of cytokinesis in animal cells. *J. Theor. Biol.* 101:289–316.

Wittmann, T., A.A. Hyman, and A. Desai. 2001. The spindle: a dynamic assembly of microtubules and motors. *Nat. Cell Biol.* 3:E28–E34.

Wolpert, L. 1960. The mechanics and mechanism of cleavage. *Int. Rev. Cytol.* 10:163–216.

Yabkowitz, R., and D.R. Burgess. 1987. Low ionic strength solubility of myosin in sea urchin egg extracts is mediated by a myosin-binding protein. *J. Cell Biol.* 105:927–936.

Yuce, O., A. Piekny, and M. Glotzer. 2005. An ECT2-centralspindlin complex regulates the localization and function of RhoA. *J. Cell Biol.* 170:571–582.

Yumura, S., and T.Q. Uyeda. 1997. Transport of myosin II to the equatorial region without its own motor activity in mitotic *Dictyostelium* cells. *Mol. Biol. Cell.* 8:2089–2099.

Zang, J.H., and J.A. Spudich. 1998. Myosin II localization during cytokinesis occurs by a mechanism that does not require its motor domain. *Proc. Natl. Acad. Sci. USA.* 95:13652–13657.

Zavortink, M., N. Contreras, T. Addy, A. Bejsovec, and R. Saint. 2005. Tum/RacGAP50C provides a critical link between anaphase microtubules and the assembly of the contractile ring in *Drosophila melanogaster*. *J. Cell Sci.* 118:5381–5392.

Zhao, W.M., and G. Fang. 2005. MgcRacGAP controls the assembly of the contractile ring and the initiation of cytokinesis. *Proc. Natl. Acad. Sci. USA.* 102:13158–13163.

Zhou, M., and Y.L. Wang. 2008. Distinct pathways for the early recruitment of myosin II and actin to the cytokinetic furrow. *Mol. Biol. Cell.* 19:318–326.